# Numerical model for confined masonry structures based on finite discrete element method

**Hrvoje Smoljanović, Nikolina Živaljić, Željana Nikolić, Ante Munjiza**

*Faculty of Civil Engineering, Architecture and Geodesy, University of Split, Split, CROATIA*
*e-mails: hrvoje.smoljanovic@gradst.hr, nikolina.zivaljic@gradst.hr, zeljana.nikolic@gradst.hr, ante.munjiza@gradst.hr*

## SUMMARY

*This paper presents a numerical model for confined masonry structures under seismic load. The model is based on a combination of the finite discrete element models for reinforced concrete confining elements and a masonry infill. Material non-linearity, including fracture and fragmentation of discrete elements, is considered through contact elements, which are implemented within a finite element mesh. The model includes the following phenomena: non-linear cyclic behaviour of concrete, reinforcement and masonry during the seismic event, interaction between the reinforcement and concrete, cracking of the reinforced concrete confining elements and masonry units, as well as failure and softening in tension and shear for mortar joints. The application of the developed numerical model is exemplified on a confined masonry wall exposed to seismic excitation.*

**KEY WORDS:** *confined masonry structures, finite-discrete element method, seismic load.*

## 1. INTRODUCTION

Confined masonry walls are often used as a structural building system in seismic active areas. Confined masonry consists of a masonry infill with reinforced concrete confining elements, which increase the stiffness and loading capacity of masonry walls. In this type of masonry, the unreinforced wall is constructed first and the confining elements later. Numerical investigation of the behaviour of confined masonry structures under seismic loading is very complex and demands precise modelling of the masonry infill, reinforced concrete elements, and their interaction during seismic event. One of the dominant causes of nonlinearity in these structures is a crack opening, which leads to a localized failure and stands out as a serious challenge in numerical modelling. Therefore, a realistic modelling of cracking is one of the key factors that enable the reliability of a model for analysis of structures of this kind, especially those affected by earthquakes.

Most of the models for simulation of the behaviour of confined masonry structures are based on the finite element method [1-3]. Since the confined masonry is a composite structure, it is

necessary to make a distinction between a numerical model for reinforced concrete confining elements and a numerical model for the masonry infill.

The main cause of non-linearity in confined masonry structure is cracking, which can be modelled with either a smeared or a discrete crack approach. Within the smeared crack approach, the local displacement discontinuities at cracks are smeared over some tributary areas within the finite element. The behaviour of cracked concrete [4, 5], or the masonry infill [6, 7], is represented by the average stress-strain relations given by the material constitutive laws. In the discrete crack approach, strong discontinuities in cracked concrete [8, 9], or between different blocks of the masonry infill [10, 11], is usually modelled with joint interface elements.

Another approach for modelling of cracking in these materials is the discrete element method [12, 13]. It is based on modelling of the concrete by elementary particles held together by cohesive forces, whereas the behaviour of masonry is based on an idealization of the material as a discontinuum where joints are modelled as contact surfaces between different blocks. Recently, an increasing number of models have attempted to combine the advantages of the finite and discrete element methods [14-16]. These methods are designed to handle contact situations in which transitions from continua to discontinua appear.

The finite discrete element method [17], the subject of this paper, was initially developed for the simulation of fracturing problems, in order to take into account deformable particles that may split and separate during an analysis. Within the framework of this method, the discrete elements are discretized by constant strain triangular finite elements. Material non-linearity, including fracture and fragmentation of discrete elements, is considered through contact elements implemented within a finite element mesh. The interaction between discrete elements is considered through the contact interaction algorithm based on the potential contact forces [18] and the Coulomb-type law for friction [19].

The finite discrete element method was successfully applied in the analysis of reinforced concrete structures [20-22] and masonry structures [23, 24] under static and dynamic load. This paper presents a numerical model for confined masonry structures under seismic load based on a combination of the finite discrete element models for reinforced concrete and masonry.

## 2. NUMERICAL MODEL OF CONFINED MASONRY STRUCTURE

In this numerical model, reinforced concrete confining elements are discretized with triangular finite elements for concrete, while reinforcing bars are modelled with linear, 1D elements. The nonlinear behaviour of concrete in tension and shear is modelled in the contact element implemented between the triangular finite elements, whereas the nonlinear behaviour of the reinforcing bar is modelled with 1D contact elements implemented between finite elements of the reinforcing bar [20, 21].
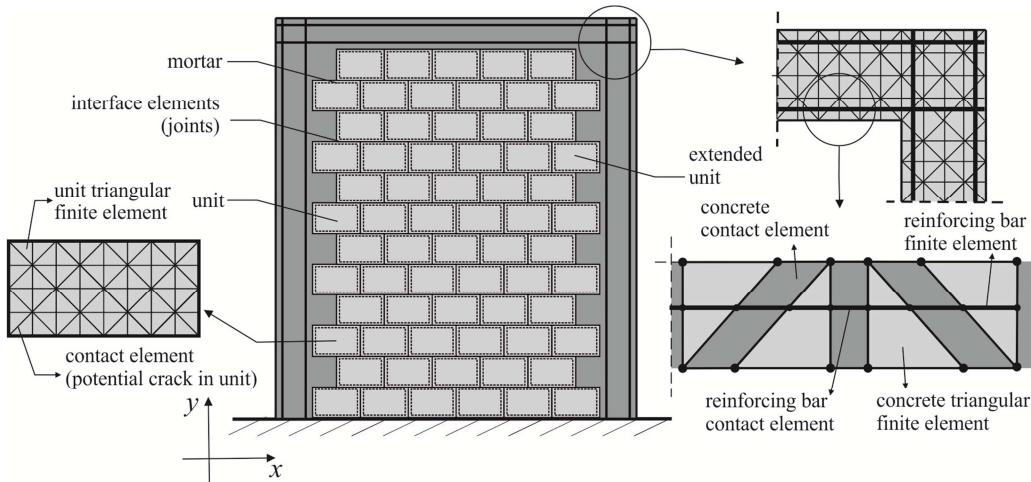
**Fig. 1** *Discretization of a confined masonry structure*

A masonry wall is considered to be an assemblage of extended unit elements connected with zero thickness interface elements, which simulate the behaviour of the mortar joints and unit-mortar interface. The extended units are discretized by triangular finite elements [23, 24]. Potential cracks in the units are considered through contact elements implemented between a finite element mesh, which is based on a combined single and a smeared crack model [18]. Discretization of a confined masonry structure is shown in Figure 1.

## 2.1 NUMERICAL MODEL OF REINFORCED CONCRETE CONFINING ELEMENTS

Discretization of the reinforced concrete confining elements with an embedded reinforcing bar is shown in Figure 1. The reinforcing bar was defined by its initial and end points. The intersection between the sides of the triangular concrete finite elements and reinforcing bars gives the reinforcement finite elements and reinforcement contact elements.

In the model presented in this paper the behaviour of concrete triangular finite element and reinforcing bar finite elements is linear elastic. Nonlinear behaviour of concrete in tension and shear is modelled in the concrete contact element. When all concrete stresses are in compressive area, crushing of concrete and nonlinear effects appears due to appearance of cracks in tension and shear which is modelled by numerical model of concrete contact elements. The nonlinear behaviour of the reinforcing bar after the appearance of the cracks in the concrete is modelled by reinforcing bar contact elements [20, 21].

Taking into account the linear-elastic relationship between stress and strain in a reinforcing bar finite element, the deformation of the reinforcing bar finite element is determined from the current and initial coordinates of the triangular finite element. This leads to forces acting in the reinforcing bar finite element nodes, which are distributed into the nodes of the parent concrete triangular element in the form of equivalent nodal forces [20, 21].

### 2.1.1 NUMERICAL MODEL OF CONCRETE CONTACT ELEMENT

The numerical model in concrete contact elements is used for the simulation of crack initiation and propagation in tension and shear [18]. The cracks are assumed to coincide with the finite element edges, which are achieved in advance through the topology of adjacent elements described by different nodes. Separation of these edges induces a bonding stress, which is

taken to be a function of the size of separation δ (Figure 2). Before reaching the tensile strength, there is no separation of element edges, which is ensured through the penalty function method [18].
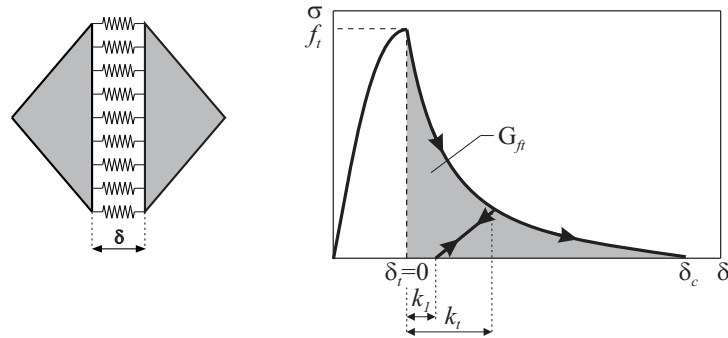
**Fig. 2** *Strain softening curve defined in terms of displacements*

After reaching a tensile strength $f_t$, stress decreases with an increasing separation $\delta$ and at $\delta=\delta_c$ bonding, the stress tends to zero. For the separation $\delta_t < \delta < \delta_c$, bonding stress is given by:

$$\sigma_c = z f_t \tag{1}$$

where $z$ is a heuristic scaling function representing an approximation of the experimental stress-displacement curves taken according to Hordijk [25]:

$$z = \left[ 1 + (c_1 D_t)^3 \right] e^{-c_2 D_t} - D_t (1 + c_1^3) e^{-c_2} \tag{2}$$

where $c_1 = 3$ and $c_2 = 6.93$, and the damage parameter $D_t$ is determined according to the following expression:

$$D_t = \begin{cases} (\delta - \delta_t)/(\delta_c - \delta_t), & \text{if } \delta_t < \delta < \delta_c; \\ 1, & \text{if } \delta > \delta_c \end{cases} \tag{3}$$

The area under the stress-displacement curve represents the energy release rate $G_{ft} = 2\gamma$, where $\gamma$ is the surface energy, i.e. the energy needed to extend the crack surface by unit area.

The same model for describing shear stress $\tau_s$ and shear displacement $t_s$ relation is adopted for concrete behaviour in shear [18].

In this paper, a numerical model in concrete contact element is extended to capture the main characteristics related to cyclic loading in tension. For this purpose, the material model shown in Figure 2 is adopted according to Reinhardt [26], where the ratio of $k_1/k_t$ was obtained experimentally from uniaxial cyclic tests and equals *0.73*.

### 2.1.2 NUMERICAL MODEL OF STEEL CONTACT ELEMENT

The model of the reinforcing bar in the contact element is divided into two parts: before and after the cracking of concrete [20].

Before the crack in concrete occurs, the continuity among the reinforcing bar finite elements is ensured through the penalty function method [20].

The numerical model of the reinforcing bar in the contact element after the cracking is based on a path-dependent mechanical model for a deformed reinforcing bar at the reinforced concrete interface as developed by Soltani and Maekawa [27]. An approximation of experimental crack opening-strain curves is used to describe the behaviour of the reinforcing

bar at crack faces. The model takes into account the bond deterioration in the reinforcement near the crack plane and can accurately account for the behaviour of a reinforcing bar that undergoes a high plastic deformation under reversed cyclic loading and shear force carried by the bar [20, 22].

After the occurrence of the crack, the axial tension force developing in the reinforcing bar is partly transferred to the concrete between adjacent cracks through bonding between the reinforcing bar and concrete. Consequently, the local stress along the bar differs from the one at the interface. It causes no uniform distribution of strains along the bar which, among other factors, depends on the bar pull out S from the crack interface (Figure 3) [22, 27].



$$(1) \quad s = \varepsilon_s(2 + 3500\varepsilon_y)$$
$$(2) \quad s = s_y = \varepsilon_y(2 + 3500\varepsilon_y)$$
$$(3) \quad s = 0.047(f_u - f_y)(\varepsilon_s - \varepsilon_{sh}) + s_y$$
$$(4) \quad s = 0.007(f_u - f_y)(\varepsilon_s - \varepsilon_{sh}) + 0.5s_y + 0.06$$
$$\varepsilon_0 = \varepsilon_{sh} + \frac{0.06 - s_y/2}{0.013(f_u - f_y)}$$
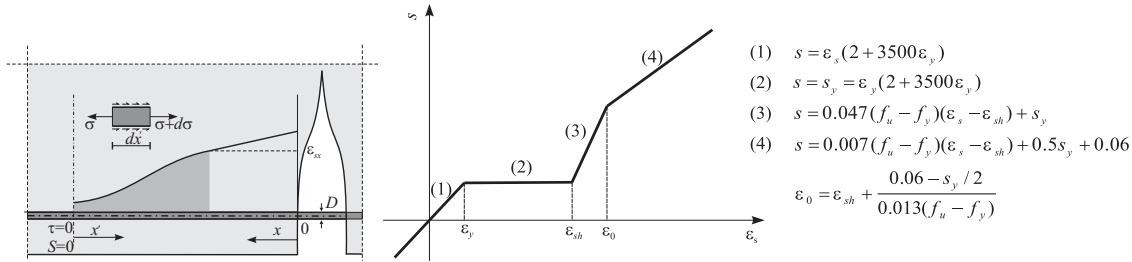
**Fig. 3** *Discrete crack and steel strain-slip relation under a monotonic loading [22]*

The monotonic slip-strain relations are defined according to a non-dimensional slip *s* given by:

$$s = \left(\frac{S}{D}\right)K_{fc}, \quad K_{fc} = \left(\frac{f_c}{20}\right)^{2/3} \tag{4}$$

where *D* is the diameter of the bar and $f_c$ is the compressive strength of concrete (MPa).

Non-dimensional slip-strain relationship before and after yielding of steel is applied according to the expressions shown in Figure 3, or in [27], where $\varepsilon_s$ represents the strain at the reinforcing bar in the crack, $\varepsilon_y$ is the yielding strain of the bar, $f_u$ and $f_y$ are the tensile strength and yield stress of steel (*MPa*) respectively, while $\varepsilon_{sh}$ is the strain at the onset of hardening. After yielding of the reinforcing bar, the normalized steel slip s is expressed as the sum of the slip $s_{pl}$ in the yield region and $s_e$ in the elastic region [27] as:

$$s = s_{pl} + s_e \tag{5}$$

Assuming a linear distribution of strain in the yield region, the normalized steel slip $s_{pl}$ is expressed as:

$$s_{pl} = \frac{(1+\beta)\varepsilon_s + \varepsilon_{sh} - \beta\varepsilon_{max}}{\varepsilon_{max} + \varepsilon_{sh}}(s_{max} - s_y) \tag{6}$$

where $\varepsilon_{max}$ and $s_{max}$ represent steel strain and non-dimensional slip immediately after the transition from loading to unloading, $\beta$ is a factor obtained from experiments and is taken as 1.0. By substituting equation (6) in (5), the strain in the reinforcing bar at the crack can be obtained from the known non-dimensional slip *s*.

The influence of adjacent cracks is approximately taken into account through a reduction factor $\alpha$ [27], which depends on an average distance between cracks $l_{cr}$. The steel slip $s_{cr}$, which considers the influence of adjacent cracks, is expressed for a monotonic loading as:

$$s_{cr} = \alpha s \tag{7}$$

where $s$ is the non-dimensional slip defined by expression (5), while the reduction factor $\alpha$ is given by:

$$\alpha = 1 - e^{-(0.065\,l_{cr}/D+0.5)^3}\,,\quad \alpha \le 0.087\,l_{cr}/D \tag{8}$$

The position of the crack is defined by a finite element edge, so the $l_{cr}$ is adopted as an input parameter, which is equal to $h/2$ where h is the concrete finite element length [20].

The stress-strain relationship for a monotonically increasing load for steel is shown in Figure 4a. The hysteresis behaviour of a steel bar is enforced through Kato's stress-strain model [28] shown in Figure 4b.
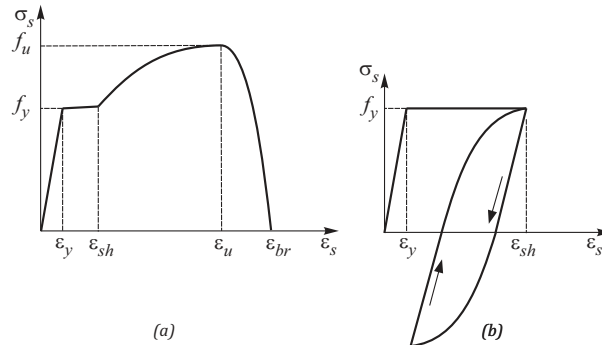


**Fig. 4** *Stress-strain model of steel: (a) monotonic loading; (b) cyclic loading [28]*

## 2.2 NUMERICAL MODEL OF MASONRY INFILL

### 2.2.1 NUMERICAL MODEL IN UNIT FINITE ELEMENT

Due to the geometrical arrangement of units and mortar, the constitutive behaviour of masonry is highly anisotropic, even if the properties of these constituents are isotropic. Oriented voids in perforated unit elements also contribute to anisotropic behaviour of masonry structures. Their material axis, in most cases, coincides with horizontal and vertical directions.

Unlike concrete structures that usually collapse due to the cracking of material in tension or shear, the material in masonry structures, besides these two failure mechanisms, often fails in compression. This failure mechanism may be especially important in masonry structures built with perforated bricks.
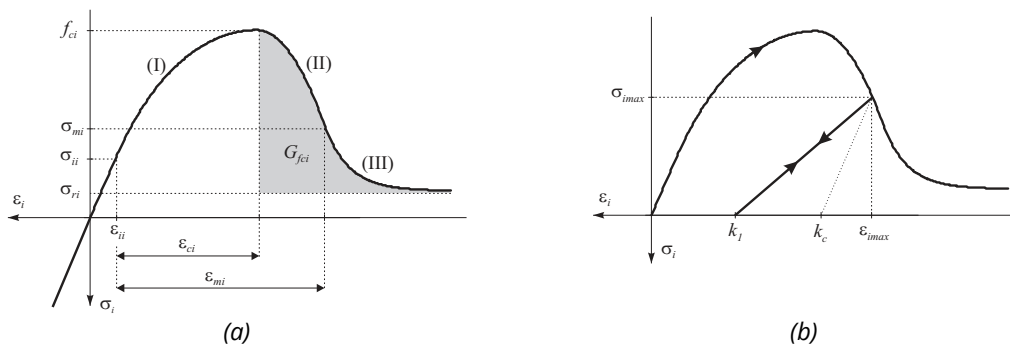


**Fig. 5** *The material model in a unit: (a) Hardening/softening law for compression; (b) Cyclic behaviour in compression [24]*

In this paper, the orthotropic constitutive material behaviour with hardening/softening law for compression is considered in finite elements [7, 23-24]. Elliptical hardening followed by a parabolic/exponential softening law in compression defined by four inelastic parameters ($\sigma_i$, $\varepsilon_i$), ($f_p$, $\varepsilon_p$), ($\sigma_m$, $\varepsilon_m$), ($\sigma_r$, $\varepsilon_r$), is shown in Figure 5a where the subscripts $i$, $m$, $c$ and $r$ denote the initial, medium, compressive peak and residual values respectively. This hardening/softening behaviour is considered for both material axes (horizontal and vertical direction), with different compressive fracture energies and different compressive strengths. A redefined compressive fracture $G_{fci}$ corresponds only to the local contribution of $\sigma_i$-$\varepsilon_i$ diagram, where subscript $i$ refers to the material axes which correspond to global axes $x$ and $y$.

Cyclic behaviour is adopted as shown in Figure 5b, where $k_1$ is the plastic strain at zero stress when unloading from monotonic tensile envelope, while $k_c$ is the plastic strain at zero stress when unloading from monotonic tensile envelope according to the initial modulus of elasticity. The ratio of $k_1/k_c$, adopted as of 0.935, is obtained from numerical analyses [24] so as to obtain the best possible correlation with the experimental results.

### 2.2.2 NUMERICAL MODEL IN INTERFACE ELEMENT

A numerical model in an interface element simulates the behaviour of the mortar joints and a unit-mortar interface by taking into account the cracking of joints in tension and sliding along the bed or head joints in shear. Since the contact elements describe discontinuity in a displacement field after reaching the ultimate tension or shear strength, their behaviour is described in terms of the relation between stress and relative displacement based on a single and smeared crack model [18]. When the relative displacement exceeds the critical displacement, interface elements fall of and contact interaction between fragmented parts is considered according to potential contact forces taking into account the Coulomb dry friction model [19].

Since the experimental research conducted by Van der Pluijm[31] has shown that increasing the pre-compression stress levels in the contact between the block and the mortar causes increasing of the fracture energy in shear, in the presented model, this phenomenon is taken into account according to the following relation:

$$G_f^{II} = G_{f0}^{II} - C\sigma \quad (N/m) \tag{9}$$

where $G^{II}_{f0}$ is the value of the fracture energy in shear in the case when the normal pre-compression stress is equal to zero, $C$ is constant in m, while $\sigma$ is a pre-compression stress in MPa. In the presented numerical model, constant $C$ is taken to be *106.31 m* [23] in order to obtain the best correlation possible with the experimental results obtained by Van der Pluijm [31].

## 2.3  PERFORMANCE OF THE PROPOSED MODEL UNDER UNIAXIAL LOADING

Considering that confined masonry structures consist of three different materials, the performance of the proposed models for masonry and confining elements, consisting of concrete and reinforcement, was validated in different cases of monotonic and cyclic tests. After having run the mentioned tests, the structure was analysed in its integrated form.

### 2.3.1 UNIAXIAL CYCLIC LOADING IN CONCRETE CONTACT ELEMENTS

The ability of the model to capture the main features of cyclic tensile tests is verified against the experimental results of Gopalaratnam and Shah [30] on concrete specimens. The cyclic loading is achieved through a controlled displacement.

The comparison between the experimental and numerical results obtained by FDEM is shown in Figure 6. The experimental data was modified in order to express a ($\sigma$-$\Delta u$) relation. The numerical response demonstrates close agreement with the experimental results.
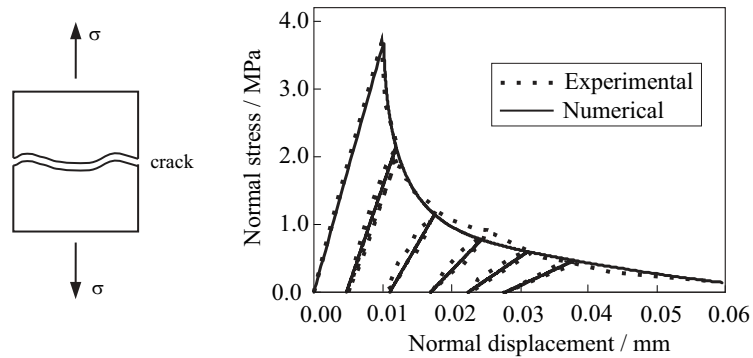


**Fig. 6** *Comparison of experimental and numerical results due to uniaxial cyclic loading in tension for: $f_t$=3.85 MPa, $G_{ft}$=100 N/m*

### 2.3.2 BEHAVIOUR OF THE STEEL CONTACT ELEMENT UNDER CYCLIC LOADING

An experimentally tested reinforced concrete beam under cyclic load [20, 27], was used to demonstrate show the performance of the numerical model in reinforcing bar contact under large inelastic cyclic loading conditions of the reinforcing bars in crack interface. In this example the cyclic loading was achieved by time-controlled displacement at end of the beam. The geometry and finite element mesh of the beam and reinforcing bars are shown in Figures 7a and 7b. In experiment [27], the crack position was pre-specified by making notches at *300 mm* intervals. In order to achieve cracks at the same places as in the experiment, a finite element mesh with implemented contact elements at the places of notches was used in the numerical analysis (Figure 7a). The concrete structure was discretized into 16 triangular elements and each reinforcing steel bar was modelled with 8 two-node elements. Modulus of elasticity of concrete $E_c$ was equal to 29000 MPa, and the compressive strength $f_c$ was *29 MPa*. Material characteristics of steel are shown in Table 1.

**Table 1** *Material characteristics of the steel*

| Young's Modulus | Yield stress | Ultimate stress | Strain at the onset of hardening | Reinforcement diameter |
|---|---|---|---|---|
| $E_s$ / MPa | $f_y$ / MPa | $f_u$ / MPa | $\varepsilon_{sh}$ | D / m |
| 190000 | 350 | 540 | 0.0165 | 0.019 |

Figure 7c shows the results obtained by the experiment against the presented model (FDEM). The results reveal that a force-average axial strain $\bar{\varepsilon}$ curve follows the experimental curve very accurately during the cyclic load, which is very important in the description of the loss of energy in the structure under cyclic load.
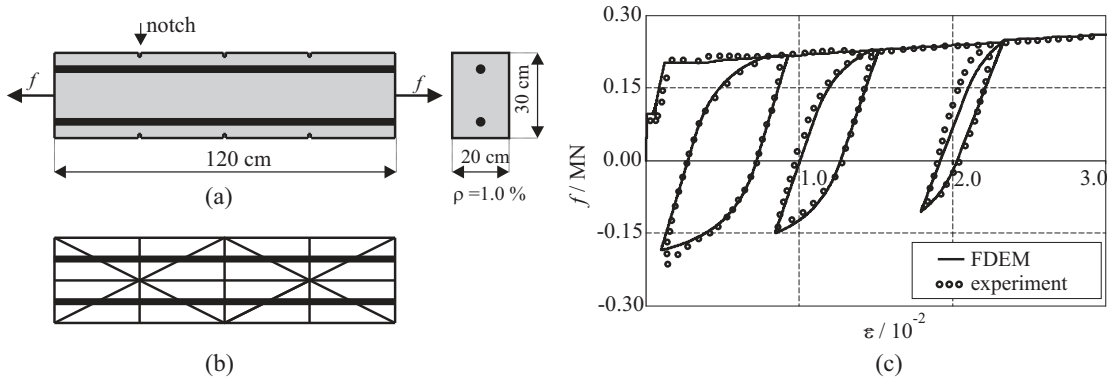
**Fig. 7** *Beam characteristics: (a) specimen for cyclic loading test; (b) finite element mesh and reinforcing bars of the beam; (c) force – average axial strain relation*

### 2.3.3 MONOTONIC TENSILE AND SHEAR BEHAVIOR IN MASONRY INTERFACE ELEMENTS

The ability of the model to capture the main features related to tensile and shear behaviour of joints under monotonic loading was checked against the experimental results. Tensile behaviour of the presented model in the interface element was compared with the experimental results obtained by Van der Pluijm [29] and are shown in Figure 8. It can be seen that the curve used in the presented numerical model for concrete proposed by Hordijk [25] correlates well with the experimental results describing the tensile softening in a mortar-block interface [24].
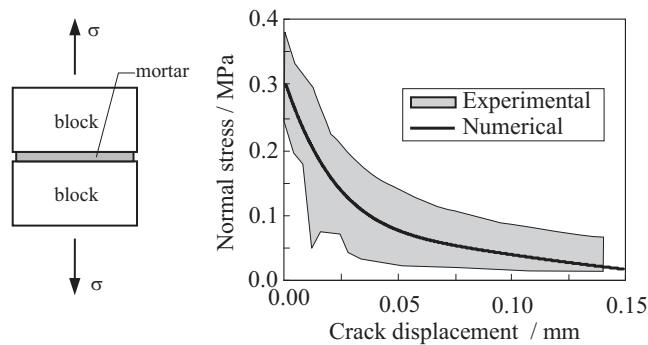


**Fig. 8** *Numerical results in comparison with the experimental behaviour [30] of unit-mortar interface in direct tension for $f_s$=0.30 MPa, $G_{If}$=12 N/m*

Direct shear tests on mortar joints for three different pre-compression stress levels carried out by Van der Pluijm [31] were used to evaluate the ability of the model to predict the shear behaviour under monotonic loading. The comparison between the experimental and numerical results is shown in Figure 9. It can be seen that the assumption of the exponential softening also seemed to be appropriate for shear monotonic loading.
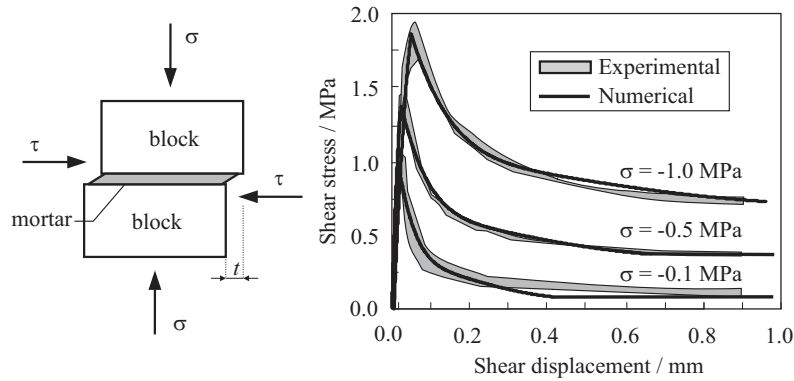
**Fig. 9** *Numerical results [23] in comparison with experimental behaviour [31] of unit-mortar interface in direct shear for $f_s$=0.87 MPa, $\mu_0$=1.01, $\mu_r$=0.73*

### 2.3.4 CYCLIC TENSILE AND SHEAR BEHAVIOUR IN MASONRY INTERFACE ELEMENTS

The ability of the model to capture the main features of the tensile and shear behaviour of the masonry interface under a cyclic loading was subsequently checked against the experimental results.

A direct shear test on mortar joints, carried out by Atkinson et al. [32], was used in this research to evaluate the ability of the numerical model of interface elements in predicting the cyclic shear behaviour in joints. The experiment was conducted on a specimen constituted of masonry blocks, with dimensions of *208 x 100 x 64 mm*, interfaced by a *7 mm* thick mortar layer. After applying a constant compressive stress of *0.33 MPa*, the specimen has been subjected to a prescribed shear displacement history varying in the range from *-12.3 mm* to *12.6 mm*.

The comparison between experimental and numerical results [24] is shown in Figure 10.
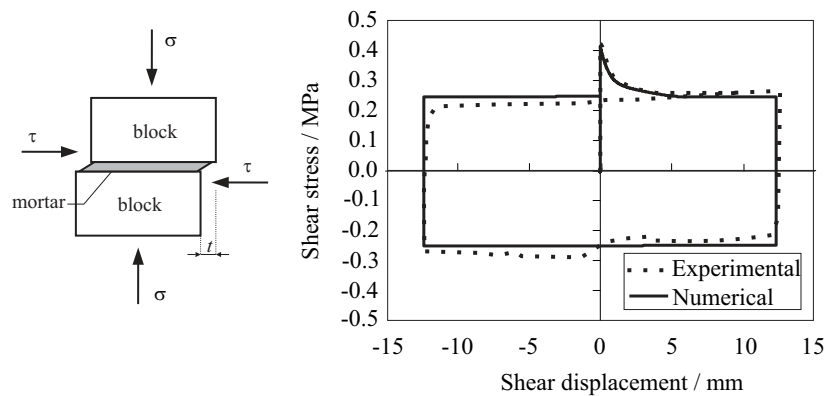


**Fig. 10** *A comparison of experimental and numerical results of direct shear test under a cyclic loading $f_s$=0.17 MPa, $G_{fs}$=147 N/m, $\mu_0 = \mu_r$=0.7 [24]*

The experimental and numerical results exhibit good agreement. It is likewise visible that the assumed elastic behaviour in shear loading/unloading approximates the experimental results quite well.

### 2.3.5 BEHAVIOUR OF THE MASONRY UNIT FINITE ELEMENT UNDER MONOTONICALLY INCREASING COMPRESSION LOAD

The implemented numerical model for a monotonically increasing compression load was validated by comparing numerical results with the experimental results obtained on four masonry prisms subjected to a uniaxial compressive stress [33]. Geometrical characteristics of the prisms are shown in Figure 11. Mechanical characteristics of the materials used in the numerical analysis are based on the data taken from the literature [33]. An average modulus of elasticity of prisms, $E_x=E_y$, was *4100 MPa*, the Poisson coefficient was *0.2*, while the compression strength $f_{cx} = f_{cy}$ and fracture energy $G_{fcx}=G_{fcy}$ were *27.5 MPa* and *23000* respectively.
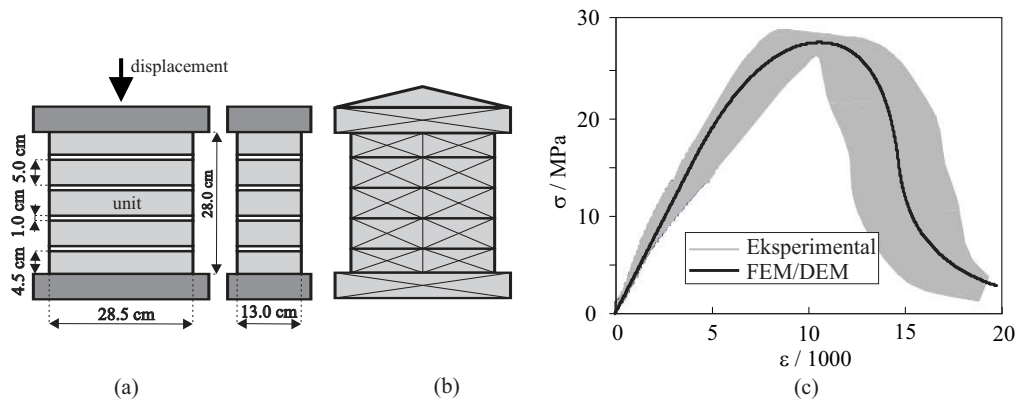


**Fig. 11** *A masonry prism: (a) geometry; (b) finite element mesh; (c) a comparison of experimental and numerical results for a monotonically increasing load in compression*

The comparison of the numerical results obtained in this paper and the experimental results obtained by Oliveira [33] are shown in Figure 11. The experimental and numerical results are shown to be in close agreement.

## 3. NUMERICAL EXAMPLE OF CONFINED MASONRY WALL

A finite discrete element model for the simulation of the dynamic response of a structure was applied to a confined masonry wall with the geometry and discretization illustrated in Figure 12. The wall thickness was equal to *0.25 m*. The wall had the constrained boundary condition at the base.
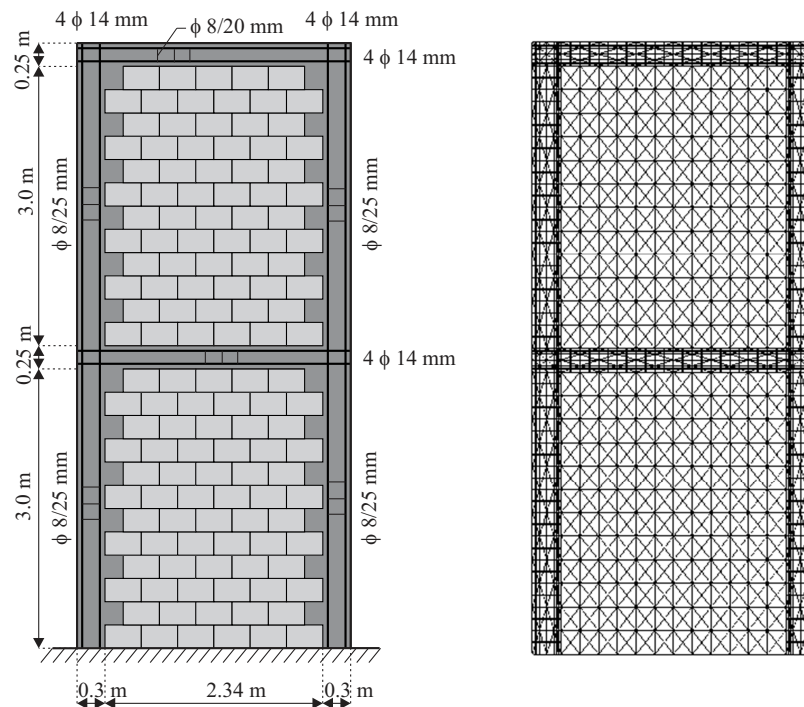
**Fig. 12** *The geometry and discretization of a confined masonry wall*

The material characteristics of the wall are given in Tables 2 and 3. A vertical load of *125 kN/m* (*0.5 MPa)* was applied on horizontal reinforced confining elements of each storey. This load consists of the weight of *20 cm* thick reinforced concrete plate with area of *7.0 m x 5.0 m*, additional dead load of *2.0 kn/m²* and imposed variable load of *3.0 kN/m²* at floor slab.

**Table 2** *Material characteristics of reinforced concrete elements*

| Concrete | | | | |
|---|---|---|---|---|
| Modulus of elasticity $E_c$ / MPa | Tensile strength $f_t$ / MPa | Compressive strength $f_u$ / MPa | Fracture energy $G_f$ / (N/m) | Spatial weight $\gamma$ (kN/m³) |
| 210 000 | 500 | 650 | 150 | 25.0 |
| **Steel** | | | | |
| Young's Modulus $E_s$ / MPa | Yield stress $f_y$ / MPa | Ultimate stress $f_u$ / MPa | | |
| 210 000 | 500 | 650 | | |

**Table 3** *Material characteristics of unit and interface elements*

| Unit | | | | |
|---|---|---|---|---|
| Modulus of elasticity $E_x=E_y$/ MPa | Poisson ratio | Compressive strength $f_{cx}$/ MPa | Compressive strength $f_{cy}$/ MPa | Spatial weight $\gamma$ (kN/m³) |
| 1033 | 0.141 | 2.7 | 10.33 | 10.0 |
| **Interface element** | | | | |
| Tensile strength $f_t$ / MPa | Shear strength $f_s$ / MPa | Fracture energy in tension $G_{ft}$ / (N/m) | Fracture energy in shear $G_{fs}$ / (N/m) | |
| 0.16 | 0.224 | 12 | 50 | |
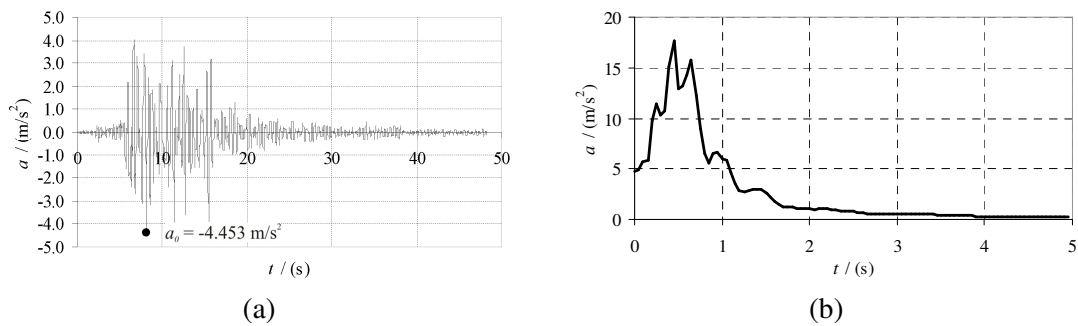
**Fig. 13** *Petrovac earthquake (1979 Montenegro): (a)Horizontal ground acceleration; (b) Elastic response spectra*

The wall was exposed to horizontal ground acceleration (Figure 13a) recorded on 15 April 1979 in Dubrovnik, on a rock soil during an earthquake with the epicentre in Petrovac, Montenegro. The acceleration was applied and increased gradually until the collapse of the structure. Corresponding elastic response spectra of the earthquake is shown in Figure 13b.

Crack initiation and propagation of the wall for ground acceleration of $a_g$=3.0 m/s² and $a_g$=4.0 m/s² are shown in Figures 14 and 16 respectively, while the displacements of the first and second stories are shown in Figures 15 and 17 respectively.

For the ground acceleration of *3.0 m/s², the* crack opening started in the vertical concrete confined elements at the bottom of the wall. For the ground acceleration of *4.0 m/s²* significant cracks at the first floor have appeared, both in units and in vertical and horizontal reinforced concrete confined elements. The maximal displacement of the top of the wall was *40 mm*, which is equal to *H*/150 where *H* is the total height of the wall.



*(a)* *(b)* *(c)*
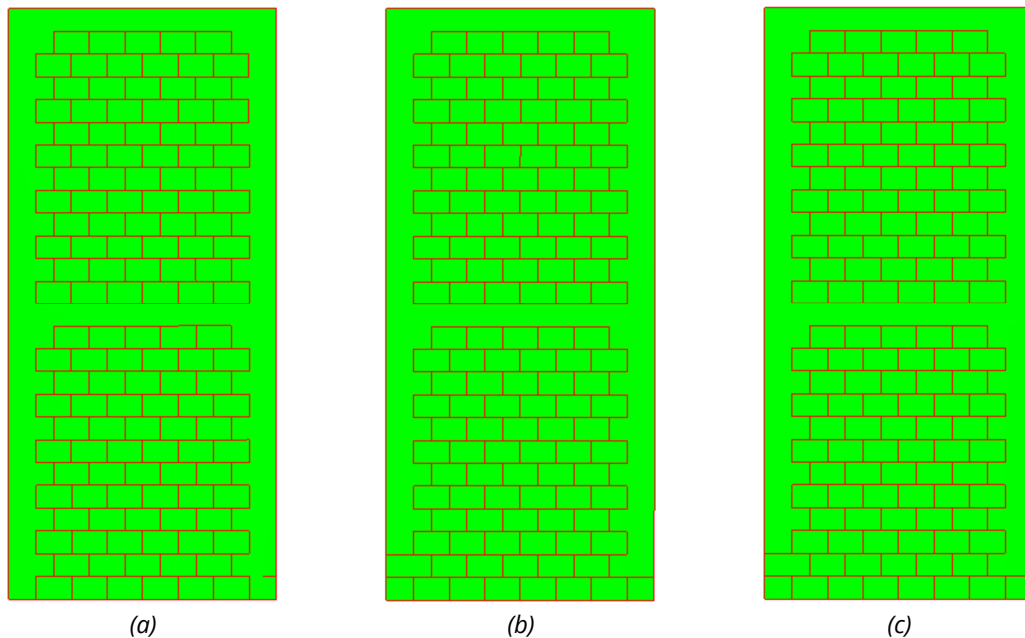
**Fig. 14** *Crack initiation and propagation for $a_g$=3.0 m/s²: (a) t=1.97 s; (b) t=7.12 s; (c) t=12.00 s*
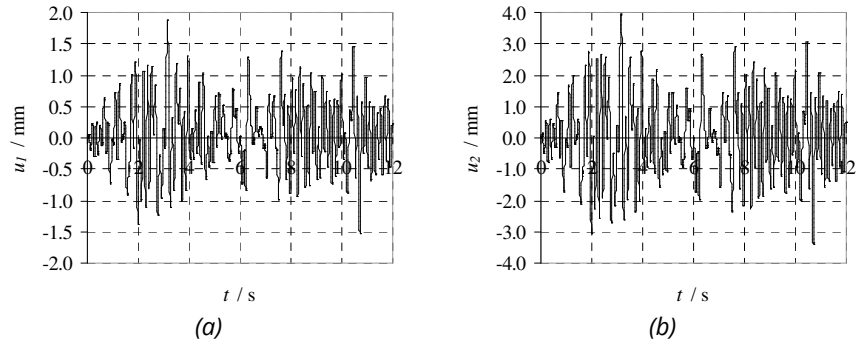
**Fig. 15** *Displacement history for $a_g$=3.0 m/s$^2$: (a) first story (b) second story*
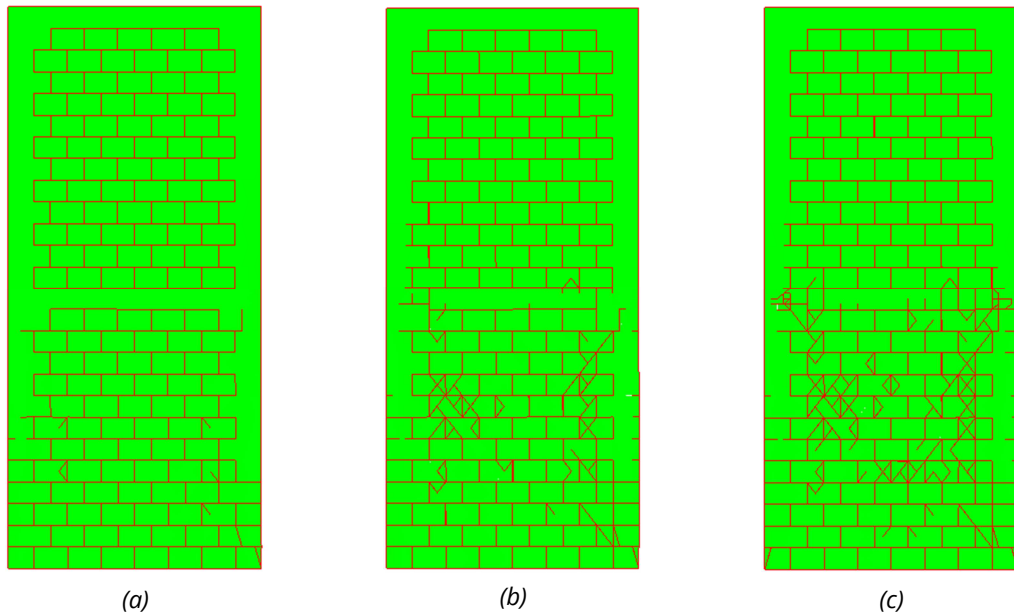


**Fig. 16** *Crack initiation and propagation for $a_g$=4.0 m/s$^2$: (a) t=4.85 s; (b) t=8.75 s; (c) t=12.00 s*
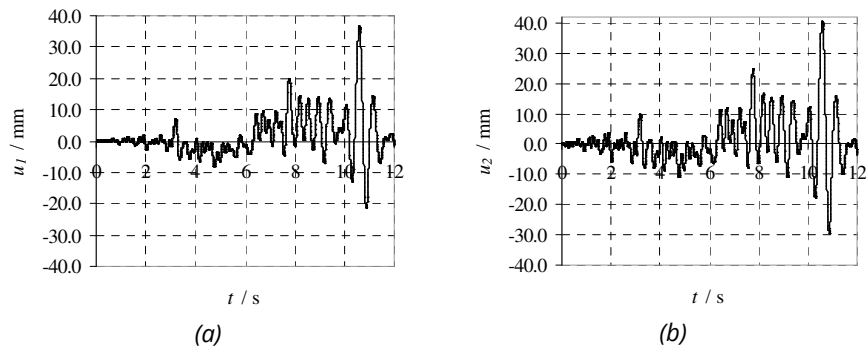


**Fig. 17** *Displacement history for $a_g$=4.0 m/s$^2$: (a) first story (b) second story*

Figure 18 shows the displacement of the top of the wall $u/H$ in relation to the ground acceleration obtained by an incremental dynamic analysis. It can be seen that the collapse of the wall was achieved during the acceleration of *4.0 m/s$^2$* when the displacement of the top of the wall was *$u/H$ = 0.67%.*
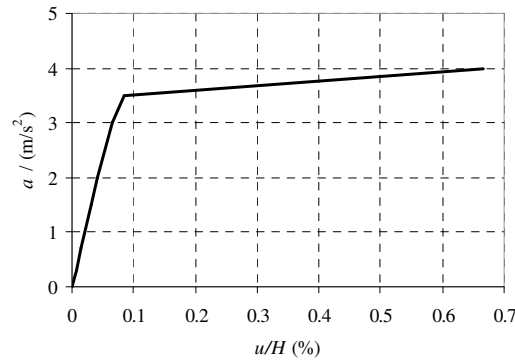
**Fig. 18** *The maximal displacement of the top of the wall in relation to the peak ground acceleration*

Generally, it can be concluded that the reason for the collapse of the walls was crushing under diagonal compression, resulting in a sudden loss of lateral resistance.

## 4. CONCLUSION

This paper presents a new numerical model for the analysis and prediction of the collapse of confined masonry structures. The presented numerical model is a synthesis of a previously developed numerical model for analysis of reinforced concrete structures and a numerical model for analysis of unreinforced masonry structures based on the finite discrete element method.

Considering that confined masonry structures consist of two different materials, reinforced concrete confining elements and a masonry infill, the performance of the proposed model was validated in different cases of monotonic and cyclic tests by comparing available experimental results with the obtained numerical results. The model demonstrates a high accuracy in predicting the behaviour of uniaxial cyclic loading between crack surfaces in concrete, behaviour of steel under cyclic loading in the crack, monotonic and cyclic tensile and shear behaviour in the mortar joints, as well as behaviour of a masonry prism under a monotonically increasing compression load.

The advantage of the presented model lies in its ability to simulate the behaviour of a confined masonry structure through the entire failure mechanism, from the continuum to the discontinuum. The example of a two-story confined masonry wall exposed to seismic excitation highlights the ability of the developed model (based on finite discrete element method) to simulate crack initiation and propagation in a realistic manner, as well as to obtain the ultimate acceleration, which is very important in the estimation of the safety of confined masonry structures under seismic loading. However further research are necessary in order to calibrate the presented numerical model with experimental results of some tested confined masonry wall.

## 5. ACKNOWLEDGEMENTS

## 6. REFERENCES

[1] P. Medeiros, G. Vasconcelos, P.B. Lourenço, J. Gouveia, Numerical modelling of non-confined and confined masonry walls, *Construction and Building Materials*, Vol. 41, pp. 968-976, 2013.

[2] S. Eshghi, K. Pourazin, In-plane behavior of confined masonry walls – with and without opening, *International Journal of Civil Engineerng*, Vol. 7, No. 1, pp. 49-60, 2009.

[3] H. Okail, A. Abdelrahman, A. Abdelkhalik, M. Metwaly, Experimental and analytical investigation of the lateral load response of confined masonry walls, *HBRC Journal*, Vol. 12, No. 1, pp. 33-46, 2016.

[4] P.H. Feenstra, R. de Borst, A composite plasticity model for concrete, *International Journal of Solids and Structures*, Vol. 33, pp. 707-730, 1996.

[5] E. Onate, S. Oller, J. Oliver, J. Lubliner, A constitutive model for cracking of concrete based on the incremental theory of plasticity, *Engineering Computation*, Vol. 5, pp.309-319, 1988.

[6] L. Pela, M. Cervera, P. Roca, An orthotropic damage model for the analysis of masonry structures, *Construction and Building Materials*, Vol. 41, pp. 957-67, 2012.

[7] P.B. Lourenço, Computational strategies for masonry structures [dissertation], Delft: Delft University of Tehnology, 1996.

[8] A. Hillerborg, M. Modeer, P.E. Petersson, Analysis of crack formation and crack growth in concrete by means of fracture mechanics and finite elements, *Cement and Concrete Research*, Vol. 6, No. 6, pp. 773-781, 1976.

[9] X.P. Xu, A. Needleman, Numerical simulations of dynamic crack growth along an interface, *International Journal of Fracture*, Vol. 74, No. 4, pp. 289–324, 1996.

[10] C. Calderini, S. Lagomarsino, Continuum model for in-plane anisotropic inelastic behaviour of masonry, *Journal of Structural Engineering*, Vol. 134, No. 2, pp. 209-20, 2008.

[11] P.B. Lourenço, J.G. Rots, A multi-surface interface model for the analysis of masonry structures, *Journal of the Engineering Mechanics ASCE*, Vol. 123, pp. 660-8, 1997.

[12] G.T. Camacho, M. Ortiz, Computational modelling of impact damage in brittle materials, *International Journal of Solids Strictures*, Vol. 33, pp. 2899–2938, 1996.

[13] M. Ortiz, A. Pandolfi, Finite-deformation irreversible cohesive elements for three-dimensional crack-propagation analysis, *International Journal for Numerical Methods in Engineering*, Vol. 44, pp. 1267–1282, 1999.

[14] A. Munjiza A, D.R.J. Owen, N. Bićanić, A combined finite-discrete element method in transient dynamics of fracturing solids, *Engineering Computations*, Vol. 12, pp. 145–174, 1995.

[15] CJ. Pearce, A. Thavalingam, Z. Liao, N. Bićanić, Computational aspects of the discontinuous deformation analysis framework for modelling concrete fracture, *Engineering Fracture Mechanics*, Vol. 65. pp. 283–298, 2000.

[16] A. Kucerova, D. Brancherie, A. Ibrahimbegovic, J. Zeman, Z. Bittnar, Novel anisotropic continuum-discrete damage model capable of representing localized failure of massive structures. Part II: Identification from tests under heterogeneous stress field, *Engineering Computations*, Vol. 26, No. 1/2, pp. 128-144, 2009.

[17] A. Munjiza, The combined finite-discrete element method, John Wiley & Sons, 2004.

[18] A. Munjiza, K.R.F. Andrews and J.K. White, Combined single and smeared crack model in combined finite-discrete element method, *International Journal for Numerical Methods in Engineering*, Vol. 44, pp. 41-57, 1999.

[19] J. Xiang, A. Munjiza, J.P. Latham, R. Guises, On the validation of DEM and FEM/DEM models in 2D and 3D, *Engineering Computations*, Vol. 26, pp. 673-687, 2009.

[20] N. Živaljić, H. Smoljanović, Ž. Nikolić, A combined finite-discrete element model for RC structures under dynamic loading, *Engineering computations*, Vol. 30, pp. 982-1010, 2013.

[21] N. Živaljić, Ž. Nikolić, H. Smoljanović, Computational aspects of the combined finite-discrete element method in modelling of plane reinforced concrete structures, *Engineering fracture mechanics*, Vol. 131, pp. 669-686, 2014.

[22] Ž. Nikolić, N. Živaljić, H. Smoljanović, Numerical modelling of reinforced-concrete structures under seismic loading based on the finite element method with discrete inter-element cracks, *Earthquake Engineering & Structural Dynamics*, Vol. 46, No. 1, pp. 159-178, 2017.

[23] H. Smoljanović, Seismic analysis of masonry structures with finite-discrete element method, Ph.D. dissertation (in Croatian), Croatia, University of Split, 2013.

[24] H. Smoljanović, Ž. Nikolić, N. Živaljić, A combined finite-discrete numerical model for analysis of masonry structures, *Engineering fracture mechanics*, Vol. 136, pp. 1-14, 2015.

[25] D.A. Hordijk, Tensile and tensile fatigue behaviour of concrete – experiments, modelling and analyses, *Heron*, Vol. 37, No. 1, pp. 3-79, 1992.

[26] H.V. Reinhardt, Fracture mechanics of an elastic softening material like concrete, *Heron*, Vol. 29, No. 2, pp. 3-41, 1984.

[27] M. Soltani and K. Maekawa, Path-dependent mechanical model for deformed reinforcing bars at RC interface under coupled cyclic shear and pullout tension, *Engineering structures*, Vol. 30, pp. 1079-1091, 2008.

[28] B. Kato, Mechanical properties of steel under load cycles idealizing seismic action, Structural concrete under seismic actions, AICAP-CEB symposium, Vol. 132, pp. 7-27, 1979.

[29] R. Van der Pluijm, Material properties of masonry and its components under tension and shear, In Neis VV, ed. Canadian Masonry Symposium: Proceedings of the 6th Canadian Masonry Symposium, Saskatoon, Saskatchewan, Canada, pp. 675-686, 1992.

[30] V.S. Gopalaratnam, S.P. Shah, Softening response of plain concrete in direct tension, *ACI Journal*, Vol. 82, pp. 310-323, 1985.

[31] R. Van der Pluijm, Shear behaviour of bed joints, In Hanid AA, Harris HG, eds. North American Masonry Conference: Proceedings of the 6th North American Masonry Conference, Philadelphia, Pennsylvania, USA, pp. 125-136, 1993.

[32] R.H. Atkinson, B.P. Amadei, S. Saeb, S. Sture, Response of masonry bed joints in direct shear, *Journal of Structural Engineering*, Vol. 115, No. 9, pp. 2276-2296, 1989.

[33] D.V. Oliveira, Experimental and numerical analyses of blocky masonry structures under cyclic loading [dissertation], Portugal, University of Minho, 2003.